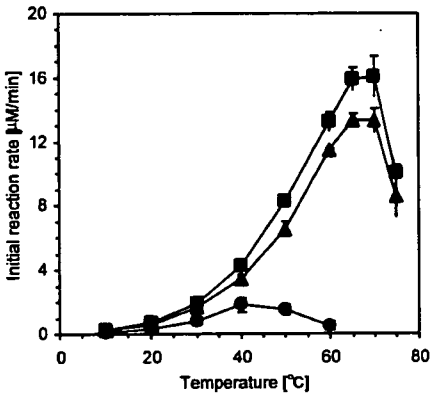

Figure 3. Temperature dependence of the enzymatic reaction of native trypsin (●) and trypsin incorporated into nonreduced (▲) and reduced (■) micelles. (Trypsin concentration 4.2 μM; substrate concentration 1.25 mM. The plots are presented as the average of three experiments ± SD.)

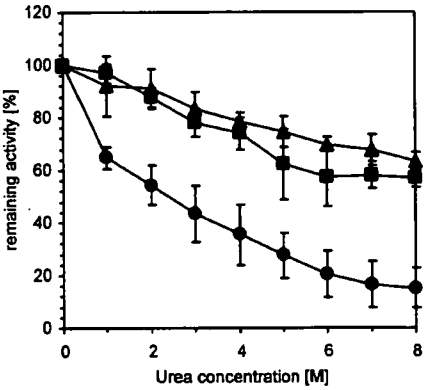

Figure 4. Change in relative remaining activity with urea concentration for native trypsin (●) and trypsin incorporated into nonreduced (▲) and reduced (■) micelles. (Trypsin concentration 16.8 μM; substrate concentration 5.0 mM; The initial reaction rates of native trypsin and trypsin incorporated into nonreduced and reduced micelles were 4.3 ± 0.1, 7.3 ± 0.7, and 8.9 ± 0.9 μM/min, respectively. The plots are presented as the average of three experiments ± SD.)

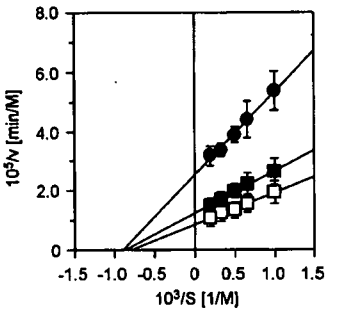

Figure 5. Lineweaver–Burk plots of native trypsin (●) and trypsin incorporated into the nonreduced (■) and reduced (□) micelles. (Trypsin concentration 16.8 μM; temperature 25 °C; $n = 3$.)

micelle. For the stabilized enzymes physically or chemically immobilized in polymer networks, the decreased enzymatic activity through the immobilization was often observed, which was induced by the restriction of the mobility of enzyme as well as by the limited solute transfer (*16*, *17*). No decrease in enzymatic activity of trypsin in the micelles might be due to the unique characteristics of core-cross-linked micelles including small size and core–shell structure with enzyme molecules stably entrapping into the core surrounded by a biocompatible and hydrophilic shell layer, providing a uniform distribution of stabilized enzymatic nanoreactor and maintenance of substrate diffusion.

The entrapment of trypsin into the micellar cross-linked core induced a substantial shift in the optimal temperature of the enzymatic reaction, as compared to native trypsin. Figure 3 shows the temperature dependence of the enzymatic reaction rate of both the native trypsin and the trypsin incorporated into the nonreduced and reduced micelles. In the case of native trypsin, a maximum reaction rate was observed at 40 °C, and this reaction rate gradually decreased in the higher-temperature region due to thermal denaturation. Obviously, the optimal temperature of the trypsin activity increased from 40 to 65 and 70 °C, respectively, for the nonreduced and reduced micelles. Various types of trypsin stabilized by polymers have been evaluated on their thermal stability, and the highest optimal temperature of stabilized trypsin in such a way was 65 °C reported by Fernandez et al. (*18*, *19*). In their study, trypsin conjugated with the derivatives of cyclodextrin showed an increased optimal temperature of trypsin, but the autolysis reaction was not completely prevented. The significant increase in the optimal temperature up to 70 °C obtained in the present study of the PIC micelle system might be due to the effective stabilization of the trypsin molecule by the introduction of the cross-linked structure in the matrix of the micellar core. In the core of the cross-linked micelles, cross-linkages were formed not only between the trypsin–trypsin molecules, but also between the primary amino groups at the ω-end of the PAA segments and the aldehyde groups in glutaraldehyde, i.e., trypsin–trypsin and trypsin–polymer cross-linkages, forming a hybrid nanogel structure. Consequently, the thermal-denaturing temperature of trypsin shifted to a higher temperature through the immobilization into the nanogel network, thus avoiding the thermal unfolding of the protein structure. It is worth noting that, in the immobilized trypsin in the micellar core, the spatial arrangement of the Asp-His-Ser catalytic triad in the trypsin molecule should be maintained even at 70 °C.

The stabilized spatial arrangement of the catalytic triad in the core-cross-linked micelles was also supported by the results of the tolerated trypsin activity against urea addition. Figure 4 shows the change in the relative remaining activity, defined as the ratio of the initial enzymatic reaction rate in the presence and absence of urea. Urea is well-known as a strong breaker of hydrogen bonding, as well as a disruptor of hydrophobic interaction, including enzyme denaturation in a concentration dependent manner. Indeed, the relative remaining activity of native trypsin gradually decreased with increasing urea concentration, and became lower than 50% at 3.0 M urea. On the other hand, even at 8.0 M urea, the trypsin incorporated into the core-cross-linked micelles maintained more than 60% of its relative remaining activity, indicating that the spatial arrangement of the catalytic triad in the cross-linked micelles was preserved even at high urea concentration. These results shown in Figures 3 and 4 suggest that the original tertiary structure of the trypsin molecule in the micelles might be effectively stabilized through chemical cross-linking.

As seen in Figures 2 and 3, the trypsin incorporated into the core-cross-linked micelles always showed higher initial reaction rates compared with native trypsin, suggesting that the enzyme incorporated into core-cross-linked micelles exhibits apparently enhanced activity. In order to evaluate the difference in the amidase activity of native trypsin and trypsin in the nonreduced and the reduced micelles, enzymatic reaction constants were determined by preparing Lineweaver–Burk plots (Figure 5). The good linear relations observed between the reciprocals of the initial reaction rate and the substrate concentration in the Lineweaver–Burk plots was confirmed not only for native

Table 1. Enzymatic Reaction Constants of Native Trypsin and Trypsin Incorporated into the Core-Cross-Linked Micelles

	k_{cat} [min^{-1}]	K_m [mM]	k_{cat}/K_m [M^{-1} min^{-1}]
native trypsin	0.236 (1.0)[a]	1.11 (1.0)[a]	213 (1.0)[a]
trypsin in nonreduced micelle	0.482 (2.0)[a]	1.14 (1.0)[a]	423 (2.0)[a]
trypsin in reduced micelle	0.689 (2.9)[a]	1.23 (1.1)[a]	560 (2.6)[a]

[a] These values were relative values against the values of native trypsin.

trypsin, but also for the trypsin incorporated into the reduced and nonreduced micelles. This linear relation indicates that the enzymatic function of trypsin incorporated into the core-cross-linked micelles can be kinetically analyzed on the basis of the Michaelis−Menten equation. The obtained enzymatic reaction constants, the catalytic rate constant (k_{cat}), the Michaelis constant (K_m), and k_{cat}/K_m, were summarized in Table 1. It was observed that the K_m values remained almost unchanged following the incorporation of trypsin into the core-cross-linked micelles, indicating that the affinity between trypsin and the substrate did not change. On the other hand, the k_{cat} values of the core-cross-linked micelles were approximately two to three times higher than that of native trypsin. The higher reaction rates of trypsin in the core-cross-linked micelles, as compared to those of native trypsin, were ascribed to an increase in the k_{cat} values. It is well-known that trypsin has a catalytic site constituted of the Asp-His-Ser triad (*20*−*22*). In this catalytic site, the nucleophilicity of the hydroxyl group of Ser increases through a proton-transfer process in the Asp-His dyad, in which the carboxylate group of Asp stabilizes the imidazolium ion of the His residue. We recently found that a part of the carboxylate group of the Asp residue in PEG-PAA stabilized an imidazolium ion of the His residue in the catalytic triad, thus accelerating the catalytic reaction of trypsin (*23*). This effect might also be induced in the core-cross-linked micelles as a means to increase the catalytic constant, as compared to native trypsin.

CONCLUSION

Core-cross-linked PIC micelles, prepared from trypsin and PEG-PAA, were effectively formed in both a reduced and a nonreduced state, both entrapping trypsin in the core. Both a remarkable improvement in the storing stability and a significant increase in the optimal temperature of the trypsin activity, as well as the marked resistance to denaturation by urea, were all confirmed as effects of the incorporation of trypsin into the core-cross-linked micelles. Note that there were few reports on the immobilization method of enzymes which attained increases in both the enzymatic activity and the optimal temperature. Most of the conventional enzyme-immobilized systems showed an apparent decrease in enzymatic activity due to the mass-transfer effect attributed to the restricted mobility of the enzyme as well as to the limited diffusion of the solute molecules (*16*, *17*). In the case of the core-cross-linked micelles, the enzymes were fixed to each other by the cross-linking reagent to form a nanoscopic hydrogel domain consisting of several tens of enzyme molecules. Since the size of the domain was sufficiently small, the diffusion of the substrate might not be the rate-determining step of the enzyme reaction. As a result, the mass-transfer effect was not significant for the core-cross-linked micelles. This is also an advantage of the cross-linked PIC micelle systems when compared to the conventional immobilization of enzymes in gel matrices with significantly larger dimensions. These core-cross-linked micelles incorporating enzymes represent a new entity of supramolecular nano-bioconjugates, which are expected to find significant application in both the medical and bioengineering fields.

ACKNOWLEDGMENT

This study was supported by the Industrial Technology Research Grant Program of the New Energy and Industrial Technology Development Organization (NEDO) of Japan.

Supporting Information Available: The quaternary pyridinium structure in the core-cross-linked micelle. This material is available free of charge via the Internet at http://pubs.acs.org.

LITERATURE CITED

(1) Griffith, L. G. (2000) Polymeric biomaterials. *Acta Mater. 48*, 263−277.

(2) Sakiyama-Elbert, S. E., and Hubbell, J. A. (2001) Functional biomaterials: design of novel biomaterials. *Annu. Rev. Mater. Res. 31*, 183−201.

(3) Vandermeulen, G. W. M., and Klok, H. A. (2004) Peptide/protein hybrid materials: enhanced control of structure and improved performance through conjugation of biological and synthetic polymers. *Macromol. Biosci. 4*, 383−398.

(4) Vriezema, D. M., Aragonès, M. C., Elemans, J. A. A. W., Cornelissen, J. J. L. M., Rowan, A. E., and Nolte, R. J. M. (2005) Self-assembled nanoreactor. *Chem. Rev. 105*, 1445−1489.

(5) Girelli, A. M., and Mattei, E. (2005) Application of immobilized enzyme reactor in on-line high performance liquid chromatography: a review. *J. Chromatogr., B 819*, 3−16.

(6) Duncan, R. (2006) Polymer conjugates as anticancer nanomedicine. *Nat. Rev. Cancer 6*, 688−701.

(7) El-Sayed, M. E. H., Hoffman, A. S., and Stayton, P. S. (2005) Smart polymeric carriers for enhanced intracellular delivery of therapeutic macromolecules. *Exp. Opin. Biol. Ther. 5*, 23−32.

(8) Alarcon, C. D. H., Pennadam, S., and Alexander, C. (2005) Stimuli responsive polymers for biomedical applications. *Chem. Soc. Rev. 34*, 276−285.

(9) Harada, A., and Kataoka, K. (2006) Supramolecular assemblies of block copolymers in aqueous media as nanocontainers relevant to biological applications. *Prog. Polym. Sci. 31*, 949−982.

(10) Harada, A., and Kataoka, K. (1998) Novel polyion complex micelles entrapping enzyme molecules in the core: preparation of narrowly-distributed micelles from lysozyme and poly(ethylene glycol)-poly(aspartic acid) block copolymer in aqueous medium. *Macromolecules 31*, 288−294.

(11) Harada, A., and Kataoka, K. (1999) On-off control of enzymatic activity synchronizing with reversible formation of supramolecular assembly from enzyme and charged block copolymers. *J. Am. Chem. Soc. 121*, 9241−9242.

(12) Harada, A., and Kataoka, K. (2001) Pronounced activity of enzymes through the incorporation into the core of polyion complex micelles made from charged block copolymers. *J. Controlled Release 72*, 85−91.

(13) Harada, A., and Kataoka, K. (2003) Switching by pulse electric field of the elevated enzymatic reaction in the core of polyion complex micelles. *J. Am. Chem. Soc. 125*, 15306−15307.

(14) Jaturanpinyo, M., Harada, A., Yuan, X., and Kataoka, K. (2004) Preparation of bionanoreactor based on core-shell structured polyion complex micelles entrapping trypsin in the core cross-linked with glutaraldehyde. *Bioconjugate Chem. 15*, 344−348.

(15) Yuan, X., Yamasaki, Y., Harada, A., and Kataoka, K. (2005) Characterization of stable lysozyme-entrapped polyion complex (PIC) micelles with crosslinked core by glutaraldehyde. *Polymer 46*, 7749−7758.

(16) Tischer, W., and Kasche, V. (1999) Immobilized enzymes: crystals of carriers? *Trends Biotechnol. 17*, 326−335.

(17) Cao, L., Langen, L., and Sheldon, R. A. (2003) Immobilized enzymes: carrier-bound of carrier-free? *Curr. Opin. Biotechnol. 14*, 387−394.

(18) Fernandez, M., Villalonga, M. L., Caballero, J., Fragoso, A., Cao, R., and Villalonga, R. (2003) Effect of beta-cycolodextrin-dextran polymer on stability properties of trypsin. *Biotechnol. Bioeng. 83*, 743−747.

(19) Fernandez, M., Villalonga, M. L., Fragoso, A., Cao, R., and Villalonga, R. (2004) Effect of beta-cyclodextrin-polysucrose poly-

mer on the stability properties of soluble trypsin. *Enzyme Microb. Technol. 34*, 78−82.

(20) Hunkapiller, M. W., Smallcombe, S. H., Whitaker, D. R., and Richards, J. H. (1973) Ionization behavior of the histidine residue in the catalytic triad of serine proteases. Mechanistic implications. *J. Biol. Chem. 248*, 8306−8308.

(21) Scheiner, S., and Lipscomb, W. N. (1976) Molecular orbital studies of enzyme activity: catalytic mechanism of serine proteinases. *Proc. Natl. Acad. Sci. U.S.A. 73*, 432−436.

(22) Craik, C. S., Roczniak, S., Largman, C., and Rutter, W. J. (1987) The catalytic role of the active site aspartic acid in serine proteases. *Science 237*, 909−913.

(23) Kawamura, A., Yoshioka, Y., Harada, A., and Kono, K. (2005) Acceleration of enzymatic reaction of trypsin through the formation of water-soluble complexes with poly(ethylene glycol)-block-poly-(α,β-aspartic acid). *Biomacromolecules 6*, 627−631.

BC070029T

Available online at www.sciencedirect.com
ScienceDirect
Reactive & Functional Polymers 67 (2007) 1361–1372
REACTIVE & FUNCTIONAL POLYMERS
www.elsevier.com/locate/react

Study of the quantitative aminolysis reaction of poly(β-benzyl L-aspartate) (PBLA) as a platform polymer for functionality materials

Masataka Nakanishi [a], Joon-Sik Park [b], Woo-Dong Jang [c], Makoto Oba [d], Kazunori Kataoka [a,b,*]

[a] *Department of Materials Engineering, Graduate School of Engineering, The University of Tokyo, 7-3-1 Hongo, Bunkyo, Tokyo 113-8656, Japan*
[b] *Center for Disease Biology and Integrative Medicine, Graduate School of Medicine, The University of Tokyo, 7-3-1 Hongo, Bunkyo, Tokyo 113-0033, Japan*
[c] *Department of Chemistry, College of Science, Yonsei University, 134 Sinchondong, Seodaemun-gu, Seoul 120-749, Republic of Korea*
[d] *Department of Clinical Vascular Regeneration, Graduate School of Medicine, The University of Tokyo, 7-3-1 Hongo, Bunkyo, Tokyo 113-8655, Japan*

Received 30 June 2007; received in revised form 31 July 2007; accepted 2 August 2007
Available online 29 August 2007

Dedicated to Professor Teiji Tsuruta on the occasion of his 88th birthday (Beiju).

Abstract

A facile and quantitative aminolysis of poly(β-benzyl L-aspartate) (PBLA) as well as the solution properties of the prepared cationic polyaspartamide were investigated in this study. The reaction was found to proceed in good yield without undesired side reactions via the formation of a succinimide intermediate in the polymer backbone, which was efficiently converted to polyaspartamide accompanying the α,β isomerization of the main chain. The polarity of solvents and the secondary structure of the polymer strand were closely related to each other in terms of reactivity and stereoselectivity. The aminolysis of PBLA treated with one equivalent amine against benzyl ester groups resulted in the complete conversion at 35 °C in random-coil solvents within 1 h. The racemization that accompanied this reaction was observed in random-coil solvents, but was efficiently suppressed in helicogenic solvents, with 95% of the optical purity maintained in CH_2Cl_2. In addition, the quantitative introduction of *N*,*N*-diisopropylethylenediamine (DIP) led to the formation of cationic polyaspartamide, poly[*N*-(*N'*,*N'*-diisopropylaminoethyl)aspartamide] (PAsp(DIP)), which showed pH and thermo-sensitivities in aqueous media. This systematic investigation of the aminolysis of PBLA with DIP demonstrates the feasibility of a PBLA-aminolysis system for designing functionalized polyaspartamides which can be useful as biomaterials.

Keywords: PBLA; Aminolysis; Quantitative side-chain reaction; Succinimide; Suppression of racemization; pH and thermo-sensitivities

* Corresponding author. Address: Department of Materials Engineering, School of Engineering, The University of Tokyo, Japan. Tel.: +81 3 5841 7138; fax: +81 3 5841 7139.
E-mail address: kataoka@bmw.t.u-tokyo.ac.jp (K. Kataoka).

1381-5148/$ - see front matter © 2007 Elsevier Ltd. All rights reserved.
doi:10.1016/j.reactfunctpolym.2007.08.009

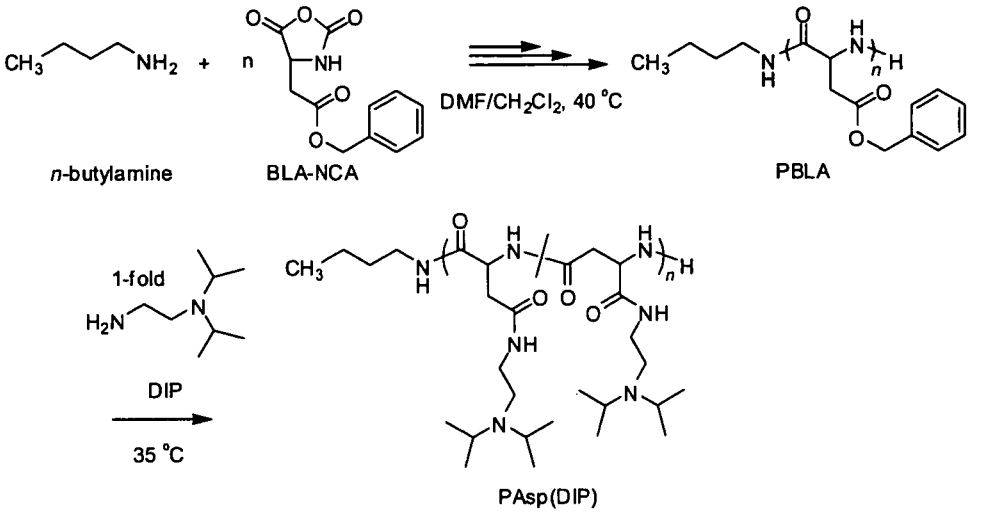

Scheme 1. Synthetic procedures of PBLA and PAsp(DIP) by the successive aminolysis reaction of PBLA.

1. Introduction

Chemical modification by the side-chain reaction of polymer is a convenient way to prepare a variety of functionalized derivatives from a single platform polymer [1–3]. For example, the precursor polymers bearing functional groups such as active ester [4–9], (meth)acryl chloride [10–12], and alkyne [13,14] are typical representatives with a potential for further functionalization or versatile modification according to particular applications. As a rule, the side-chain reaction was considered a facile synthetic route to obtaining polymer analogues with a constant degree of polymerization (DP) and molecular weight distribution (MWD) from a single platform polymer. Thus, the use of precursor polymer as a common intermediate allows for combinatorial strategies, feasible for evaluating and optimizing the correlation between the polymer structure and function.

There have also been many examples in bio-related fields where poly(amino acid)s with high biocompatibility and low toxicity [15–18] were chemically modified to increase their feasibility by binding hydrophobic drugs [19], a hydrophilic ethylene glycol segment [20] and pilot molecules [21] into the side chain. Although there have been several studies on side-chain modification using poly(lysine) or poly(glutamate/aspartate) as a platform polymer, the side-chain reaction of these poly(amino acid)s does not proceed quantitatively. The conversion of all the flanking moieties of the precursor polymers requires extreme conditions such as a high concentration of reactant, high temperature and long reaction time, leading to side reactions such as the decrease of molecular weight (MW) by the cleavage of the amide linkages in the main-chain, as in the case of the aminolysis of Poly(γ-benzyl L-glutamate) (PBLG) [22,23]. Alternatively, poly(succinimide) has been investigated as a more active precursor to preparing the isomeric library of polyaspartamide by the quantitative introduction of the functional groups [24–29]. However, the synthesis of this active precursor has some drawbacks, including a long time reaction, high reaction temperature, and coloring of the obtained product [30,31], limiting the resultant polymer under control. Namely, the polymers are still highly heterogeneous, not only in terms of DP and MWD but also in terms of optical purity and composition of the functional units in the side chain [32,33].

In this regard, we have recently established that the flanking benzyl ester groups of poly(β-benzyl L-aspartate) (PBLA) undergo a quantitative aminolysis reaction with various primary amine compounds, thus offering a variety of polyaspartamides useful for designing polymeric micelles and vesicles as a biomaterial application [34–39]. Although it has been suggested that the mechanism of this unique aminolysis reaction is involved with the succinimidyl ring formation, the details have not yet been clarified. Thus, it is critical to obtain insight into the reaction mechanism, particularly from the standpoint of kinetics, and to identify the detailed structure of polyaspartamide in order to assess its feasibility for use as biomaterials. To this aim, we investigated the mechanism and kinetics of the aminolysis reaction of PBLA, focusing on both the α to β transition

and racemization relevant to the solvent effect and the higher-ordered structure of polymer strands.

In this study, the cationic polyaspartamide was synthesized by reacting PBLA with *N,N*-diisopropylethylenediamine (DIP), and its solubility behavior responsive to pH and temperature was investigated. DIP was selected as a nucleophile to study the aminolysis mechanism and the environmentally responsive properties of polyaspartamide. The primary amino group of DIP was converted to the amide group after the aminolysis of PBLA, and the *N,N*-diisopropylaminoethyl group of DIP was responsible for pH- and thermo-sensitivities (Scheme 1). Among several alkyl groups as a hydrophobic moiety, the isopropyl group was selected with the expectation that a sharp transition of the polymer in aqueous media, like the typical thermoresponsive polymer, poly(*N*-isopropylacrylamide) [40], would occur. In addition, the tertiary amino group with two neighboring isopropyl groups was also selected not only for the hydrophobic-hydrophilic balance between the ionic segment and alkyl segment, but also to exclude undesired cross-linking during the aminolysis. Concerning the kinetics, in general the reactivity of side chains can be controlled not only by the polarity of the solvent but also by the polymer conformation depending on the solvation of side groups, steric hindrances, and the distance of the vicinal groups. From this point of view, we conducted this study in a comparable solvent system for the purpose of evaluating each effect of solvent polarity and polymer conformation on the kinetics and racemization.

2. Experimental

2.1. Materials

β-Benzyl L-aspartate *N*-carboxy-anhydride (BLA-NCA) was obtained from Nippon Oil and Fats (Tokyo, Japan). *N,N*-Dimethylformamide (DMF), 1,4-dioxane (dioxane), dimethylsulfoxide (DMSO), dichloromethane (CH_2Cl_2), and chloroform ($CHCl_3$) were purchased from Wako Pure Chemical Industries (Osaka, Japan) and were purified by distillation according to the conventional procedure [41]. *N,N*-Diisopropylethylenediamine (DIP), *n*-butylamine and triethylamine (TEA) were purchased from Tokyo Kasei Kogyo (Tokyo, Japan) and were distilled from calcium hydride under reduced pressure. The other chemicals were used as received.

2.2. Method

The ^{1}H NMR spectrum was recorded on a JEOL EX 300 spectrometer (JEOL, Tokyo, Japan) at 300 MHz. Chemical shifts were reported in parts per million (ppm) downfield from tetramethylsilane. MW and MWD were estimated using a gel-permeation chromatography (GPC) (TOSOH HLC-8220) system equipped with two TSK gel columns (TSK-gel Super AW4000 and Super AW3000) and an internal refractive index (RI) detector. The columns were eluted with *N*-methyl-pyrrolidone (NMP) containing lithium bromide (50 mM) (0.3 ml min^{-1}) at 40 °C. MW were calibrated with poly(ethylene glycol) standards (Polymer Laboratories, Ltd., UK). The IR spectra were obtained with an IR-550 JASCO spectrophotometer. Gas chromatography (GC) was carried out with GC17A (SHIMADZU, Tokyo, Japan) gas chromatograph equipped with a 30-m long, 250 μm i.d., open tubular column, DB-1 (SHIMADZU GLC, Tokyo, Japan), and a flame ionization detector. C-R7A (SHIMADZU, Tokyo, Japan) was used for instrument control and data acquisition. The carrier gas was hydrogen. The pressure at the head of the column was 400 kPa, and the linear velocity at the end of the column was 41 cm s^{-1}. The sample was injected onto the column at a split ratio of over 25:1. The injection port temperature was 200 °C.

2.3. Synthesis of poly(β-benzyl L-aspartate) (PBLA)

To obtain PBLA (Scheme 1), BLA-NCA (2.49 g, 10 mmol) was polymerized in the mixture of DMF (10.0 mL) and CH_2Cl_2 (100 mL) at 40 °C by the initiation from the terminal primary amino group of *n*-butylamine (14.6 mg, 200 μmol). PBLA was purified by precipitation in ether (3 L) three times, and was confirmed to have a unimodal MWD (M_w/M_n: 1.07) by GPC measurement (Fig. 1C). The DP of PBLA was calculated to be 52 based on ^{1}H NMR spectroscopy (Fig. 1A).

2.4. Synthesis of poly[N-(N',N'-diisopropylaminoethyl)aspartamide] (PAsp(DIP))

Lyophilized PBLA (202 mg, 20 μmol) was dissolved in DMSO (10 mL), followed by the reaction with 1-fold DIP (1 equiv to the residual benzyl ester group in PBLA, 144.3 mg, 1 mmol) under mild anhydrous conditions at 35 °C for 1 h to obtain

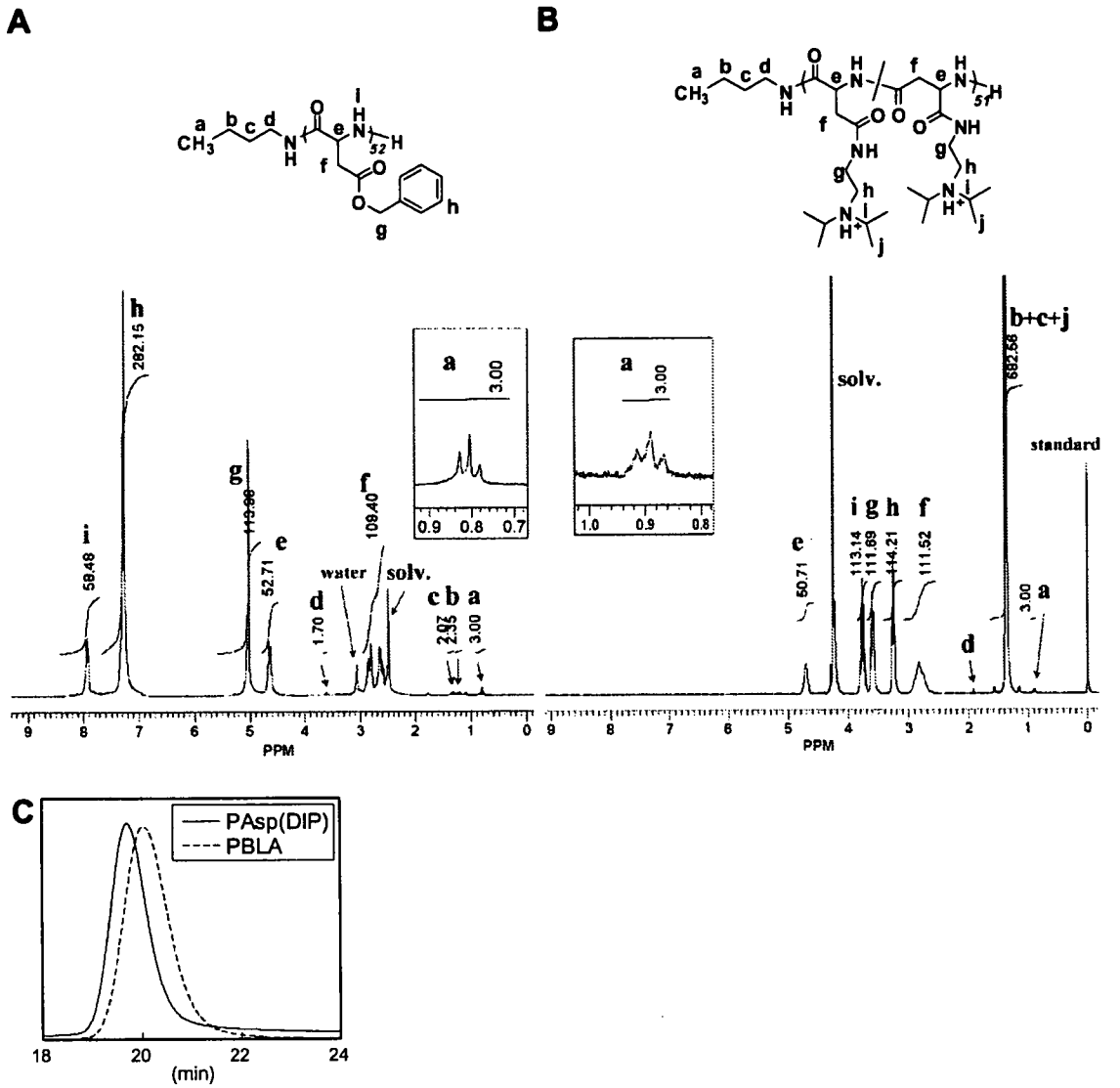

Fig. 1. ^{1}H NMR spectra of (A) PBLA in DMSO-d_6 at 50 °C and (B) PAsp(DIP) synthesized in DMSO in D_2O at 80 °C. (C) GPC diagrams of PBLA and PAsp(DIP) (PEG standard, eluent: NMP (containing 50 mM LiBr), temperature 40 °C, RI detection).

PAsp(DIP). After the reaction, the reaction mixture was slowly added dropwise into a cooled aqueous solution of acetic acid (10% v/v, 40 mL) and dialyzed against an aqueous solution of 0.01 N HCl three times and distilled water one time (molecular weight cut off: 3500 Da). The final solution was lyophilized to obtain the polymer in the chloride salt form with a yield of 92% (221 mg). In addition to the chloride salt form, the unprotonated PAsp(DIP)s were obtained as follows. The reaction mixture was purified by dialysis against DMSO three times and methanol three times. The solution was evaporated *in vacuo* and the polymer was dissolved in benzene, followed by lyophilization. The unprotonated PAsp(DIP) was then obtained as a white powder with a yield of 90% (215 mg). Similarly, the aminolysis of PBLA with DIP was carried out at 35 °C in NMP (reaction time: 1 h), DMF (reaction time: 1 h), $CHCl_3$ (reaction time: 200 h) and CH_2Cl_2 (reaction time: 160 h), respectively. In the case of dioxane, the solution of PBLA in dioxane was at first completely dissolved at 50 °C and then the temperature was allowed to decrease the temperature to 35 °C, followed by the reaction with an equivalent DIP for 260 h. All the yields were approximately 90%. The completion of the aminolysis reaction was confirmed by GC.

2.5. Reaction velocity measurements

The aminolysis of PBLA was carried out using an equivalent DIP at 35 °C in a comparable solvent sys-

tem. The conversion of the BLA residue into the aspartamide residue was calculated from both the remaining amount of DIP and the amount of the benzyl alcohol. The remaining amount of DIP was measured using GC with the internal reference method using *n*-decane as internal standard. PBLA (202 mg) was reacted with 1-fold DIP (144 mg) in 10 mL of solvent. The rate of debenzylation was determined by comparison of the intensity of CH_2 of the leaving benzyl alcohol with that of benzyl ester based on ^{1}H NMR spectroscopy using DMSO-d_6 and CD_2Cl_2 as solvent. PBLA (20.2 mg) was reacted with DIP (14.4 mg) in 1 mL of solvent at 35 °C during the ^{1}H NMR measurement.

2.6. Optical rotation measurements

The specific optical rotation measurements of the polymer samples were carried out in CH_2Cl_2 and DMSO respectively, using a digital polarimeter DIP-370 (JASCO) at a 546 nm wavelength, with a cell of 100 mm length and an integration time of 30 s. The concentration of polymer was adjusted to 1.0 wt% for all the measurements. $[\alpha]_D$ was measured at definite time intervals after adding 1-fold DIP. The measurement was done 20 times for each sample to obtain the average value.

2.7. Analysis of aspartamide enantiomers

The D/L-aspartamide ratios were determined by high performance liquid chromatography carried out by the HiPep Laboratories (Kyoto, Japan) using the enantiomer labeling method (ELAB). This analysis was conducted using a fully automated D/L and quantitative amino acid analyzer, a Shimadzu-CAT Model DLAA-1, which consists of an automated derivatizer with a robot arm, Autoderivat 100/2 of CAT, and a gas chromatograph, Shimadzu Model GC/DLAA with an auto injector, AOC/DLAA, in combination with a chromatographic data processor, Shimadzu Chromatopac C-R4A [42].

2.8. Potentiometric titration and transmittance measurements

PAsp(DIP) (30 mg) prepared in DMF was dissolved in 50 mL 0.01 N HCl and titrated with 0.01 N NaOH added in quantities of 0.063 mL after the pH values were stabilized (minimal interval: 30 s), using an automatic titrator (TS-2000, Hiranuma, Kyoto, Japan) for the titration and transmittance measurements. The pH values and transmittance were measured at 10 °C, 20 °C, 30 °C, 40 °C and 50 °C. The α/pH curves were determined from the titration curves obtained. Each calibration was carried out at the same temperature as each measurement.

3. Results and discussion

3.1. Preparation of PAsp(DIP)

PBLA is known to form the left-handed α-helix in apolar solvents such as dioxane [43], $CHCl_3$ [44], CH_2Cl_2 [45] and the random-coil in polar solvents such as DMF [46] and DMSO [43]. Because of this, these five random-coil and helicogenic solvents with various dielectric constants were selected for this study.

From the ^{1}H NMR measurement, the DP of the PAsp(DIP), comparing the peak intensity ratio of the CH_3 of the *n*-butyl group (**a**) with α-C*H* of PAsp(DIP) (**e**) was calculated to be 51, and it was confirmed that PAsp(DIP) synthesized in DMSO has a unimodal MWD (M_w/M_n: 1.08) by GPC measurement, thus indicating that the aminolysis proceeded quantitatively without causing any cleavage of the main chain (Fig. 1). Similarly, it was confirmed that all the PAsp(DIP)s prepared in other solvents had almost the same MW and a unimodal MWD (Table 1). Therefore, this result demonstrated that the aminolysis of PBLA was a useful side-chain exchanging reaction avoiding the side reaction of the cleavage of the main chain in the appropriate condition.

3.2. Reaction velocity

A significant difference was found in the reaction rate between polar random-coil solvents and apolar helicogenic solvents, as shown in Fig. 2. The reaction was much faster in random-coil solvents than in helicogenic solvents. From a practical point of view, it is worth mentioning that aminolysis with a 1-fold amine is completed after 1 h at 35 °C in polar solvents. In addition, although no difference was found in reactivity among random-coil solvents, the reaction was clearly faster in helicogenic solvents with the increasing dielectric constant of the solvent, suggesting that the rate of the aminolysis reaction of PBLA also depends on the polarity of the solvents. The results of the kinetic studies show that the aminolysis of side-

Table 1
Analytical data of M_w/M_n and L-isomer (%) of PAsp(DIP) synthesized in various solvents

Polymer solvent	PBLA	PAsp(DIP)				
		Dioxane	$CHCl_3$	CH_2Cl_2	DMF	DMSO
ε[a]		2.2	4.8	9.1	37	47
M_w/M_n[b]	1.07	1.08	1.07	1.08	1.09	1.08
L (%)[c]	99.9	83.8	89.0	94.5	72.7	73.6

[a] Indicates the dielectric constant of the solvent.
[b] Determined by GPC.
[c] Determined by ELAB method carried out by HiPep laboratories.

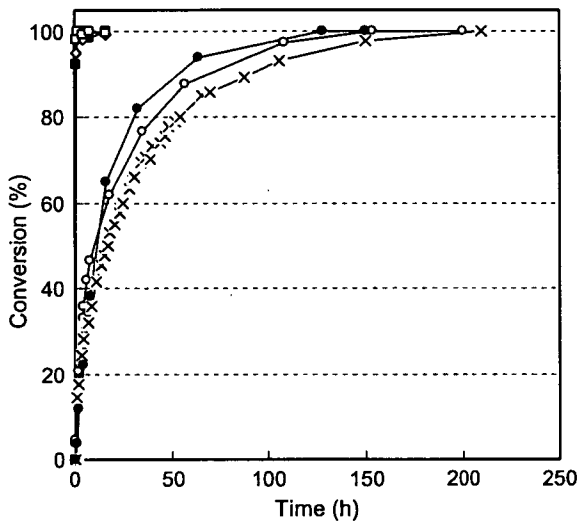

Fig. 2. Time profile of the conversion rate calculated from the remaining DIP in DMSO (□), DMF (◇), CH_2Cl_2 (○) and $CHCl_3$ (×) and the leaving benzyl alcohol in DMSO-d_6 (■) and CD_2Cl_2 (●) in the condition where PBLA reacts with 1-fold DIP at 35 °C.

chain esters of PBLA can be greatly affected by both the conformation of the polymer strand and the polarity of the solvents.

The kinetics data described above suggest that there could be an active intermediate to have this reaction progress rapidly and quantitatively, because the aminolysis of esters, in other words, a way of directly transforming esters to amides, usually requires stoichiometric amounts of promoters or metal mediators [47]. It has been reported that a large amount of primary amines was required to modify all the flanking esters in the side chain of PBLG by aminolysis, and that main-chain scission caused due to the aminolysis of the amide linkage in the main chain by the remaining primary amines [22,23]. In contrast, the stoichiometric aminolysis reaction of PBLA resulted in the prompt and complete conversion in polar and apolar solvents under a mild condition. Of interest is the significant difference in the reaction rate between PBLA and PBLG, because the difference between their primary structures is the presence or absence of γ-CH_2 in the side chain. Blout et al. [46] reported the formation of poly(succinimide), an active precursor polymer, from PBLA when PBLA was treated with catalytic amounts of base in DMF or DMSO. The formation of poly(succinimide) was determined by isolation and comparison with the infrared spectra reported in the literature [46]. However, the treatment of PBLG under identical conditions showed no evidence of cyclization to poly(glutarimide) [46]. Therefore, the mechanism by which α to β isomerization of aspartic acid occurs was focused here in order to understand the mechanism by which the aminolysis of PBLA occurs. Moreover, there have been many reports showing that the racemization of aspartic acid and asparagine residues was accelerated via succinimide intermediates [48–53]. From this result, it is highly expected that the racemization occurs when the succinimide formation occurs.

For the reasons mentioned above, it is estimated that there are three stages: (1) ring formation, (2) racemization, (3) aminolysis in the present reaction of PBLA (Scheme 2). The reaction rate constants of each stage were defined as k_1, k_2 and k_3, respectively. In the first stage, the aminolysis of PBLA starts with the activation of the nitrogen atom in the main chain by an amine as a weak base coordinating the proton of the amide group, and then the nucleophilic attack by the activated nitrogen on the carbon atom of the carbonyl group in the side chain occurs to form the succinimidyl ring. The eliminated proton which recombines with the benzyloxyl group is released as benzyl alcohol, accompanying the regeneration of amine. Therefore, the ring formation is expected to be a catalytic reaction. In the second stage, the proton in the α-position is easily eliminated with ease in the succinimidyl ring, and then racemization proceeds by the keto–enol tau-

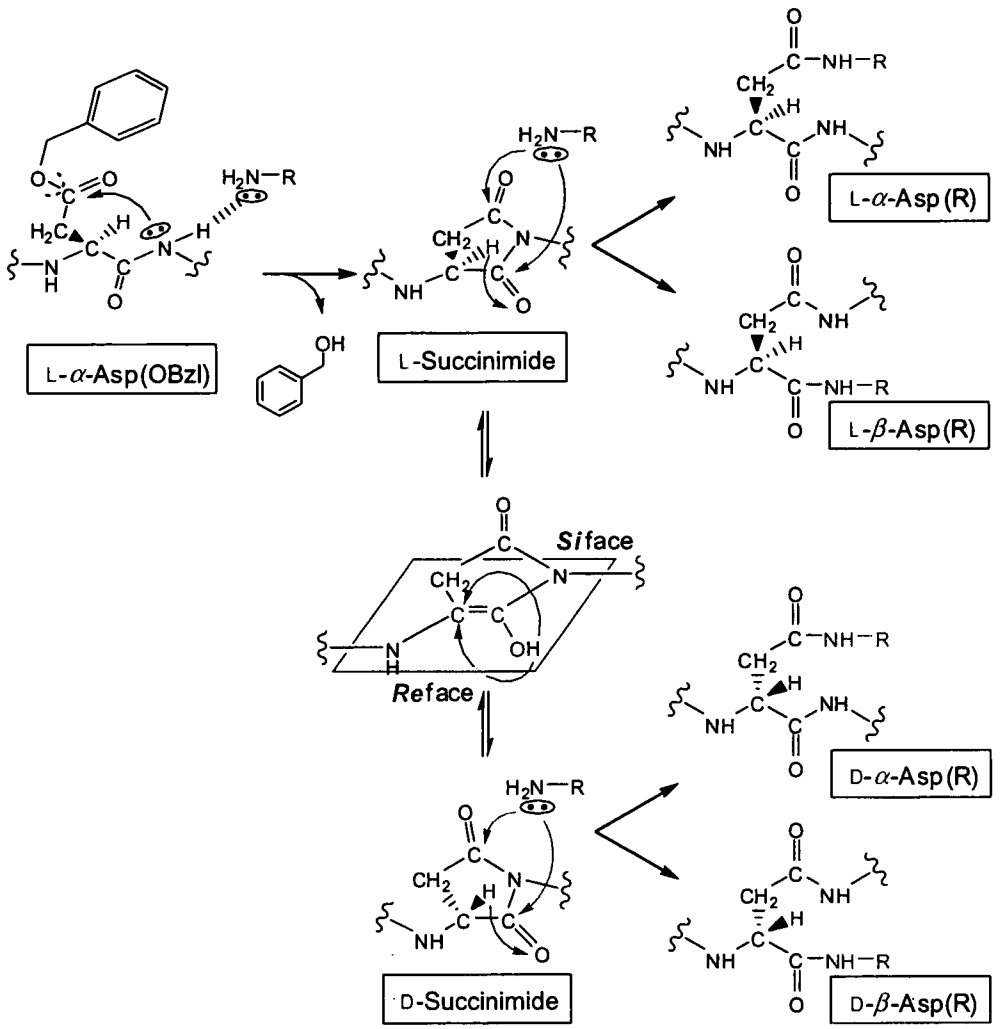

Scheme 2. Mechanism of aminolysis reaction of PBLA.

tomerism. In the third stage, an amine undergoes a nucleophilic attack to one of two carbonyl groups in the succinimidyl ring, which is efficiently converted to the isomerization to form the α,β-aspartamide.

Therefore, the aminolysis of PBLA by less than a 1-fold amount of DIP in DMSO($-d_6$) or CH_2Cl_2 (CD_2Cl_2) was performed to confirm whether aminolysis proceeds via the formation of the succinimide

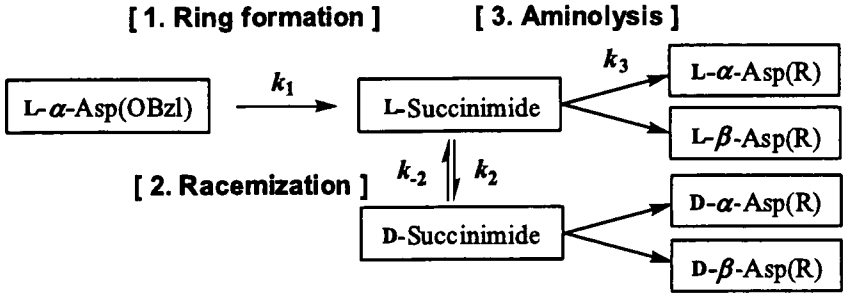

intermediate or not. In addition, the degree of racemization after the aminolysis of PBLA with 1-fold DIP was analyzed.

3.3. Identification of intermediate structure and kinetics

3.3.1. Identification of intermediate structure and kinetics in DMSO

The confirmation of an intermediate structure was done in the condition where PBLA reacted with 0.5-fold DIP in DMSO-d_6 using ^{1}H NMR spectroscopy recorded after 0.5 h, 1 h and 6 h (Fig. 3). It was determined that a 0.5-fold amount of DIP was added to this system by comparing the intensity of CH_3 (**j**) of DIP with that of CH_2 (**c**) of the benzyl group of PBLA. The sharp peak of CH_2 (**f**) of the leaving benzyl alcohol appeared at 4.5 ppm, and the intensity increased promptly in association with the separation of the peak (**d**) due to the benzyl alcohol. The integration value of CH_2 (**f**) of the benzyl alcohol became ca. 2 at 1 h. This is consistent with the complete disappearance of the peak corresponding to CH_2 (**c**) of the benzyl group of PBLA within 1 h. Thus, it was confirmed that the debenzylation was completed within 1 h. It was also confirmed by GC that all the DIP were consumed after 6 h.

Comparing the spectrum of PBLA (A) with that of the reactant at 0.5 h (B) in Fig. 3, it is worth noting the substantial shift of the α-C*H* (**a**) peak at 4.7 ppm. Concomitantly, the peak assigned to β-CH_2 seems to shift from 2.6 and 2.8 ppm (**b**) to 2.7 and 3.2 ppm (**l**), respectively, suggesting the substantial change in the main chain structure. Furthermore, the appearance of new peaks at 5.3 (**k**) and 5.1 (**m**) ppm was clearly observed. For further analysis, each intensity and the summation of the two peaks (**k**) and (**m**) from (B) to (D) in Fig. 3 were compared. According to the reported chemical shift values of poly(succinimide) [54], the peaks (**k**) and (**l**) were assigned to α-C*H* and β-CH_2, respectively, of the succinimide ring produced in the main chain. In accordance with the gradual decrease in the peak intensity of peak (**k**) with time, an alternative increase in the intensity for peak (**m**) was observed, suggesting the progress of the aminolysis reaction. Note that the summation of the peak intensities of (**k**) and (**m**) always took the constant value of 1.1 after 1 h. Therefore, it is reasonable to conclude that the peak (**m**) is assigned to α-C*H* of polyaspartamide. The time-trace of the ^{1}H NMR spectra revealed that the aminolysis reaction successively occurred after the prompt progress of succinimide formation ($k_1 > k_3$) in DMSO.

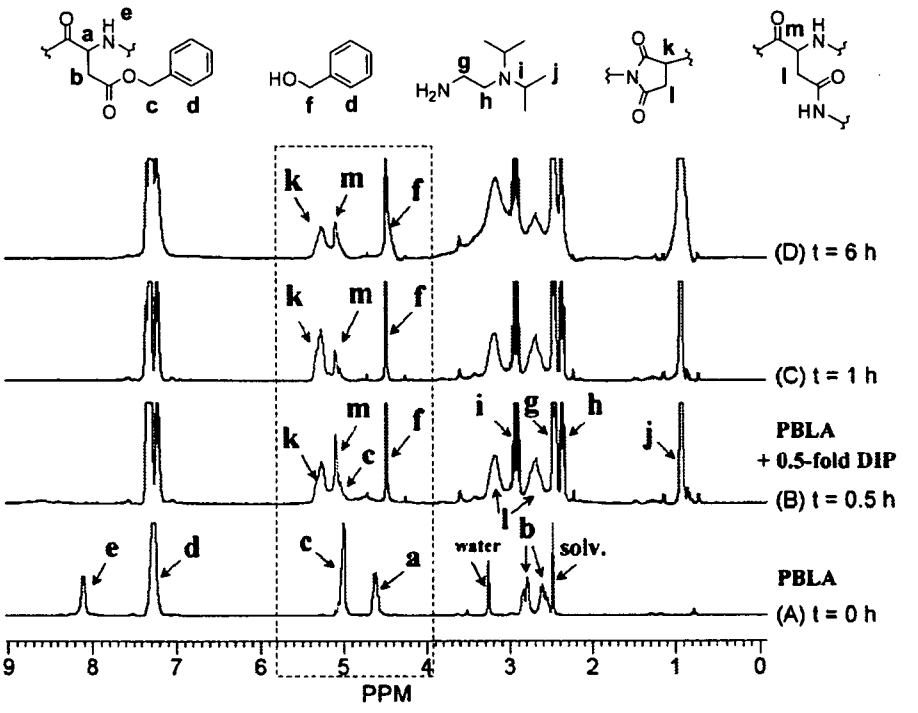

Fig. 3. Time-trace of ^{1}H NMR spectra of PBLA reacting with 0.5-fold DIP in DMSO-d_6 at 35 °C.

Next, an IR measurement was performed to directly detect the succinimide structure in the condition where PBLA reacted with 0.005-fold DIP in DMSO at 35 °C for 30 min. In the IR spectrum of the product, the amide I, amide II and ester peaks almost disappeared and the imide peaks of the succinimidyl ring appeared clearly at 1717 cm^{-1} and 1800 cm^{-1}, as shown in Fig. 4A and B. The IR spectrum of the product was very similar to that of the model imide, *N*-ethyl-succinimide (data not shown) and similar to the spectrum of Poly(succinimide) which has been reported [46]. Therefore, it is reasonable to conclude that DIP catalytically transduces the BLA residue to succinimide, an active intermediate, which then quantitatively converted to aspartamide, and that aspartamide includes β-isomer.

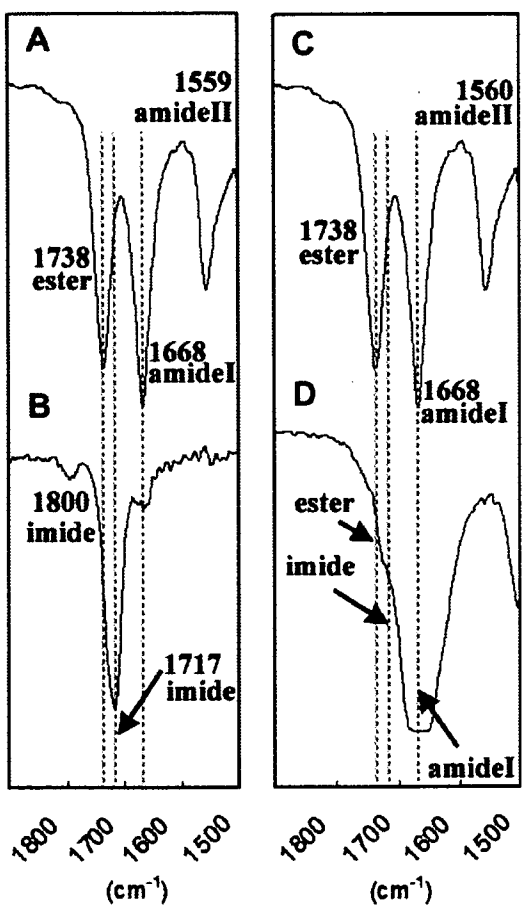

Fig. 4. Infrared absorption spectra with assignments at a range of 1800–1500 cm^{-1} of (A) PBLA, (B) PBLA reacting with 0.005-fold DIP in DMSO for 30 min, (C) PBLA reacting with 0.005-fold DIP in CH_2Cl_2 for 24 h, and (D) PBLA reacting with 1-fold TEA in CH_2Cl_2 for 12 h.

3.3.2. *Identification of intermediate structure and kinetics in CH_2Cl_2*

Similarly, the identification of an intermediate structure in CH_2Cl_2 was carried out to explore the mechanism involved in the quantitative aminolysis reaction in apolar solvents. The ^1H NMR spectra were obtained in the condition where PBLA reacted with 0.5-fold DIP in CD_2Cl_2 at 35 °C as shown in Fig. 5. The sharp peak of CH_2 (**f**) of the leaving benzyl alcohol appeared at 4.6 ppm with a gradual increase in the intensity, with the reaction time occurring more slowly than that in the DMSO-d_6 system. Eventually, 47% of benzyl alcohol was eliminated in 237 h. Nevertheless, no peak corresponding to succinimide as an intermediate structure was found in the spectra from (A) to (E), unlike in the DMSO-d_6 system. An IR measurement was carried out in the condition where PBLA reacted with the catalytic amount of DIP for 24 h in CH_2Cl_2. The spectrum obtained after 24 h was quite similar to that of PBLA (Fig. 4C) without any sign of succinimide ring formation. Further analysis was then carried out using triethylamine (TEA) as a weak base, which can act as a catalyst leading to formation of the succinimide ring, yet cannot undergo an aminolysis reaction because of the lack of a primary amino group. Eventually, the solution of PBLA reacting with an equivalent TEA for 24 h became turbid, and its IR spectrum clearly included the band assignable to the imide structure (Fig. 4D), indicating the formation of a succinimide structure.

Note that poly(succinimide) is known to be insoluble in CH_2Cl_2 [46], being consistent with the precipitate formation in the reaction mixture of PBLA with TEA in CH_2Cl_2. In the reaction system with DIP, the produced succinimide moiety promptly reacted with the primary amino group of DIP to form an aspartamide with a flanking diisopropylaminoethyl group because the succinimidyl ring formation was the rate-limiting step ($k_1 < k_3$), eventually maintaining the polymer solubility in CH_2Cl_2.

3.4. *Stereoselectivity*

A measurement of the specific optical rotation was conducted to analyze the racemization and conformational change of the polymer strand during the aminolysis of PBLA. Notably, a significant difference in $[\alpha]_D$ was observed between the polymers dissolved in DMSO and CH_2Cl_2 (Fig. 6). $[\alpha]_D$ of the polymer in DMSO immediately became almost

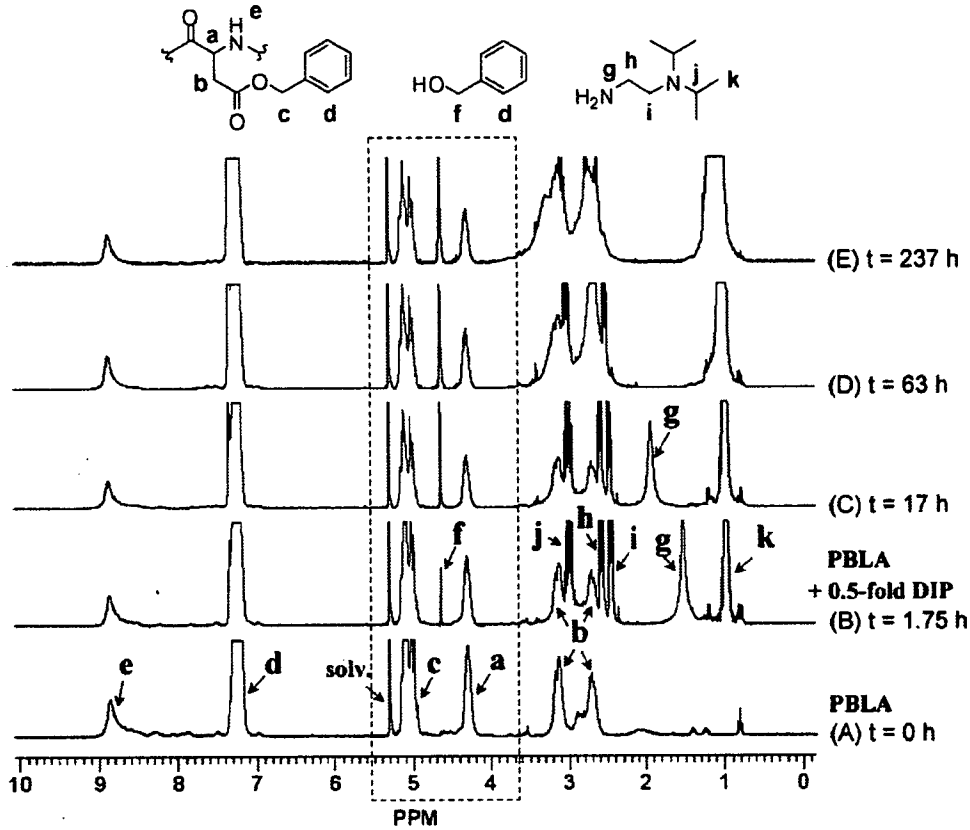

Fig. 5. Time-trace of ^{1}H NMR spectra of PBLA reacting with 0.5-fold DIP in CD_2Cl_2 at 35 °C.

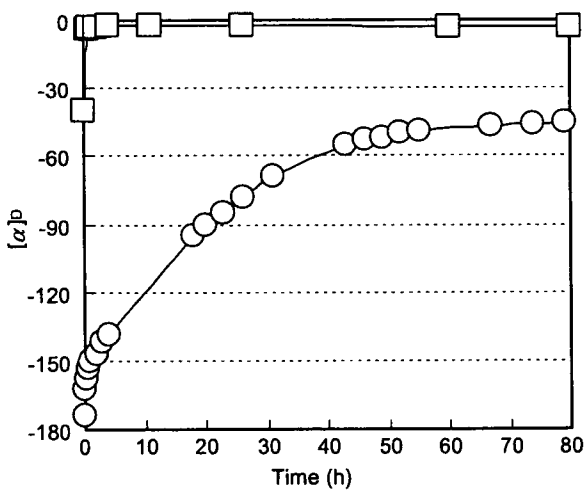

Fig. 6. Time-trace of $[\alpha]_D$ of PBLA reacting with 1-fold DIP at room temperature in DMSO (□) and CH_2Cl_2 (○).

zero after the DIP addition, suggesting the prompt racemization. $[\alpha]_D$ of PBLA in CH_2Cl_2 showed a highly negative value compared to that in DMSO due to the formation of the left-handed α-helix. Then, after the addition of DIP, alternatively, $[\alpha]_D$ of the system revealed a gradual shift in the positive direction and converged from the value of −180 to −45 after 80 h. It should be noted that the $[\alpha]_D$ value of −45 coincided with that for the random coiled PBLA in polar solvents such as DMSO.

Further analysis revealed that racemization occurred in the polar solvents and was effectively prohibited in the apolar solvents (Table 1), indicating that the $k_{2\_apolar\ solvent}$ was quite smaller than the $k_{2\_polar\ solvent}$. It is worth mentioning that the optical purity of the L-isomers was maintained with the yield of 95% in CH_2Cl_2, which is unprecedentedly high.

Racemization occurs by the rearrangement of the eliminated proton in the α position from Si face known as the keto–enol tautomerization (Scheme 2). It is reasonable to assume that the keto–enol tautomerzation is thermodynamically easy to occur in the polar solvents and not in the apolar solvents. Therefore, the racemization was effectively prohibited in the apolar solvents. Furthermore, the secondary structure of the polymer strands may also be a factor affecting racemization. The formation of an enol structure may be restricted in the α-helical structure because of the

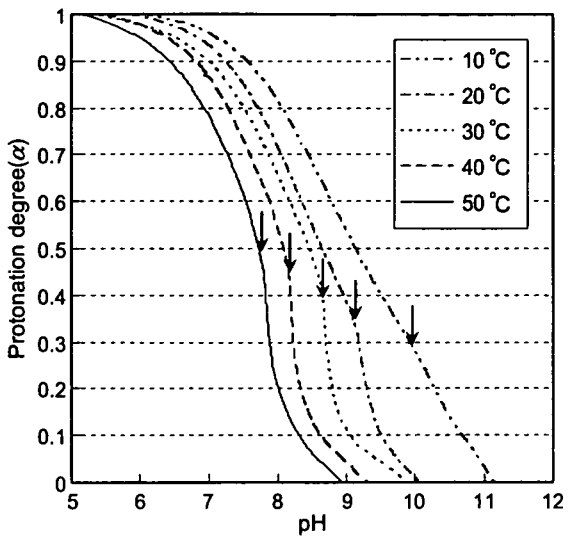

Fig. 7. Protonation degree (α) as a function of pH (α/pH curve) for PAsp(DIP) prepared in DMF. Each arrow in the figure indicates the pH at which the transmittance of the polymer solution decreased to 95%.

intramolecular hydrogen bond. However, further analyses may be needed to clearly explain the reaction scheme.

3.5. Solution properties of PAsp(DIP)

The analysis of the aqueous solution property of PAsp(DIP) synthesized in DMF was performed by the potentiometric titration and transmittance measurement to obtain α–pH curves at various temperatures (Fig. 7). The transmittance sharply decreased at a specific pH for all of the measuring temperatures, suggesting that the polymer became hydrophobic with the deprotonation to precipitate out of the solution.

The apparent pK_a ($pK_{a,app}$) values defined as a pH of $\alpha = 0.5$ increased with the decrease of the temperature from $pK_{a,app} = 7.7$ at 50 °C to $pK_{a,app} = 9.3$ at 10 °C. These results indicate that at a higher temperature, PAsp(DIP) is more liable to release proton because it is energetically preferable for the amphiphilic polycations to release highly condensed protons on the polymer strand to form the collapsed globule. However, stabilization due to the hydrophobic hydration was promoted at a lower temperature to maintain the solubility of PAsp(DIP) even at the higher range of pH. Eventually, PAsp(DIP) will be feasible to use as a novel smart materials with dual sensitivity i.e., sensitivity to both pH and temperature.

4. Conclusion

It was revealed that the aminolysis of PBLA, which proceeds involving a succinimide intermediate, was useful for quantitatively introducing the functional group into the side chain of PBLA. Moreover, racemization was effectively suppressed through the aminolysis in CH_2Cl_2 to give polyaspartamide with an appreciably high optical purity of 95%. This optical purity will apparently be a great advantage in its application as biomaterials. The cationic PAsp(DIP) synthesized by this method showed the dual sensitivity to pH and temperature, and thus may have a potential utility as novel smart biomaterials. In conclusion, this method of aminolysis is a simple and efficient way of constructing a polyaspartamide library from PBLA as a single platform polymer, and can be applied for screening the various utilities of structurally well-defined polyaspartamide derivatives as functionality materials.

Acknowledgements

The authors wish to express their gratitude to Prof. T. Tsuruta, Professor Emeritus, The University of Tokyo, for his valuable discussions and critical comments on this research. This work was financially supported by the Core Research for Evolutional Science and Technology (CREST) from the Japan Science and Technology Agency (JST).

References

[1] S. Jean-Claude, B. Jean-Claude, React. Polym. 12 (1990) 3.
[2] S. Jean-Claude, B. Jean-Claude, React. Polym. 12 (1990) 133.
[3] S. Jean-Claude, B. Jean-Claude, React. Polym. 13 (1990) 1.
[4] R. Arshdy, Adv. Polym. Sci. 111 (1994) 1.
[5] H. Mao, C. Li, Y. Zhang, S. Furyk, P.S. Cremer, D.E. Bergbreiter, Macromolecules 37 (2004) 1031.
[6] A. Godwin, M. Hartenstein, A.H.E. Müller, S. Brocchini, Angew. Chem. Int. Ed. 40 (2001) 594.
[7] W. Wu, B. Jin, G. Krippner, K. Watson, Bioorg. Med. Chem. Lett. 10 (2000) 341.
[8] L.E. Strong, L.L. Kiessling, J. Am. Chem. Soc. 121 (1999) 6193.
[9] A. Carrillo, K. Gujraty, P. Rai, R. Kane, Nanotechnology 16 (2005) S416.
[10] P. Strohriegl, Makromol. Chem. 194 (1993) 363.
[11] Y.S. Yang, G.R. Qi, J.W. Qian, S.L. Yang, J. Appl. Polym. Sci. 68 (1998) 665.
[12] Y.X. Liu, Z.J. Du, Y. Li, C. Zhang, C.J. Li, X.P. Yang, H.Q. Li, J. Appl. Polym. Sci. 44 (2006) 6880.
[13] R. Luxenhofer, R. Jordan, Macromolecules 39 (2006) 3509.

[14] B. Parrish, R.B. Breitenkamp, T. Emrick, J. Am. Chem. Soc. 127 (2005) 7404.
[15] T.J. Deming, Adv. Drug. Deliv. Rev. 54 (2002) 1145.
[16] S. Brocchini, Adv. Drug. Deliv. Rev. 53 (2001) 123.
[17] M. Ali, S. Brocchini, Adv. Drug. Deliv. Rev. 58 (2006) 1671.
[18] A. Lavasanifar, J. Samuel, G.S. Kwon, Adv. Drug. Deliv. Rev. 54 (2007) 169.
[19] G. Pratesi, G. Savi, G. Pezzoni, O. Bellini, S. Penco, S. Tinelli, F. Zunino, Brit. J. Cancer 52 (1985) 841.
[20] H.J.-P. Ryser, W.-C. Shen, Proc. Natl. Acad. Sci. USA 75 (1978) 3867.
[21] G.Y. Wu, C.H. Wu, J. Biol. Chem. 262 (1987) 4429.
[22] N. Lupu-Lotan, A. Yaron, A. Berger, M. Sela, Biopolymers 3 (1965) 625.
[23] A.D. Marre, H. Soyez, E. Schacht, J. Pytela, Polymer 35 (1994) 2443.
[24] M.G. Meirim, E.W. Neuse, F. Parisi, Angew. Makromol. Chem. 175 (1990) 141.
[25] E.W. Neuse, A.G. Perlwitz, S. Schmitt, Angew. Makromol. Chem. 181 (1990) 153.
[26] E.W. Neuse, A.G. Perlwitz, S. Schmitt, Angew. Makromol. Chem. 192 (1991) 35.
[27] E.W. Neuse, B.B. Patel, C.W.N. Mbonyana, J. Inorg. Organomet. Polym. 1 (1991) 147.
[28] J.C. Swarts, E.W. Neuse, G.J. Lamprecht, J. Inorg. Organomet. Polym. 4 (1994) 143.
[29] R.W. Niven, F. Rypacek, P.R. Byron, Pharm. Res. 7 (1990) 990.
[30] M. Schwamborn, Polym. Degrad. Stab. 59 (1998) 39.
[31] K.C. Low, A.P. Wheeler, L.P. Koskan, Adv. Chem. Ser. 248 (1996) 99.
[32] T. Nakato, M. Yoshitake, K. Matsubara, M. Tomida, T. Kakuchi, Macromolecules 31 (1998) 2107.
[33] S.K. Wolk, G. Swift, H.-P. Yi, K.M. Yocom, R.L. Smith, E.S. Simon, Macromolecules 27 (1994) 7613.
[34] K. Itaka, N. Kanayama, N. Nishiyama, W.-D. Jang, Y. Yamasaki, K. Nakamura, H. Kawaguchi, K. Kataoka, J. Am. Chem. Soc. 126 (2004) 13612.
[35] S. Fukushima, K. Miyata, N. Nishiyama, N. Kanayama, Y. Yamasaki, K. Kataoka, J. Am. Chem. Soc. 127 (2005) 2810.
[36] Y. Bae, W.-D. Jang, N. Nishiyama, S. Fukushima, K. Kataoka, Mol. Biosyst. 1 (2005) 242.
[37] A. Koide, A. Kishimura, K. Osada, W.-D. Jang, Y. Yamasaki, K. Kataoka, J. Am. Chem. Soc. 128 (2006) 5988.
[38] N. Kanayama, S. Fukushima, N. Nishiyama, K. Itaka, W.-D. Jang, K. Miyata, Y. Yamasaki, U.-I. Chung, K. Kataoka, Chem. Med. Chem. 1 (2006) 439.
[39] Arnida, N. Nishiyama, N. Kanayama, W.-D. Jang, Y. Yamasaki, K. Kataoka, J. Control. Release 115 (2006) 208.
[40] H.G. Schild, Prog. Polym. Sci. 17 (1992) 163.
[41] D.D. Perrin, W.L.F. Armarego, D.R. Perrin, Purification of Laboratory Chemicals, Pergamon, Oxford, 1980.
[42] K. Nokihara, J. Gerhardt, Chirarity 13 (2001) 431.
[43] P. Dubin, F.E. Karasz, Biopolymer 11 (1972) 1745.
[44] R.H. Karlson, K.S. Norland, G.D. Fasman, E.R. Blout, J. Am. Chem. Soc. 82 (1960) 2268.
[45] E.R. Blout, Biopolymers Symp. 1 (1964) 397.
[46] A.J. Adler, G.D. Fasman, E.R. Blout, J. Am. Chem. Soc. 85 (1963) 90.
[47] C.G. Swain, J.F. Brown, J. Am. Chem. Soc. 74 (1952) 2538.
[48] J.L. Radkiewicz, H. Zipse, S. Clarke, K.N. Houk, J. Am. Chem. Soc. 118 (1996) 9148.
[49] G.G. Smith, G.V. Reddy, J. Org. Chem. 54 (1989) 4529.
[50] T. Takata, T. Shimo-Oka, K. Miki, N. Fujii, Biochem. Biophys. Res. Commun. 334 (2005) 1022.
[51] N. Fujii, K. Harada, Y. Momose, N. Ishii, M. Akaboshi, Biochem. Biophys. Res. Commun. 263 (1999) 322.
[52] N. Fujii, L.J. Takemoto, Y. Momose, S. Matsumoto, K. Hiroki, M. Akaboshi, Biochem. Biophys. Res. Commun. 265 (1999) 746.
[53] A.C.T. Van Duin, M.J. Collins, Org. Geochem. 29 (1998) 1227.
[54] T. Nakato, A. Kusuno, T. Kakuchi, J. Polym. Sci. Part A: Polym. Chem. 38 (2000) 117.

CHEMMEDCHEM

DOI: 10.1002/cmdc.200700076

Enhanced Growth Inhibition of Hepatic Multicellular Tumor Spheroids by Lactosylated Poly(ethylene glycol)-siRNA Conjugate Formulated in PEGylated Polyplexes

Motoi Oishi,[a] Yukio Nagasaki,*[a, c] Nobuhiro Nishiyama,[d] Keiji Itaka,[d] Motoki Takagi,[e] Akira Shimamoto,[e] Yasuhiro Furuichi,[e] and Kazunori Kataoka*[b, d]

PEGylated polyplexes (lac-PEGylated polyplexes) composed of poly(L-lysine) and lactosylated poly(ethylene glycol)-small interfering RNA conjugate, which inhibits the RecQL1 gene product, were revealed to show an appreciable growth inhibition of multicellular HuH-7 spheroids (human hepatocarcinoma cell lines) for up to 21 days (IC_{50}=6 nM); this system used as an in vitro three-dimensional (3D) model mimicking the in vivo biology of tumors. The PEGylated polyplexes thus prepared had a size of approximately 110 nm with clustered lactose moieties on their periphery as targeting ligands for the asialoglycoprotein-receptor-expressing HuH-7 cells. In contrast, OligofectAMINE/siRNA (cationic lipoplex) was observed to have almost no growth-inhibitory effect against HuH-7 spheroids, even though the lipoplex showed a stronger growth-inhibitory effect than the lac-PEGylated polyplexes on conventional monolayer-cultured HuH-7 cells. The FITC-tagged conjugate in the lac-PEGylated polyplexes showed smooth penetration into the HuH-7 spheroids compared with that in the lipoplexes, as observed by confocal fluorescence-scanning microscopy. This indicates that the small size of approximately 100 nm and the reduced nonspecific interaction due to the nonionic and hydrophilic lactosylated PEG layer contributes to the smooth penetration of the PEGylated polyplexes into the spheroid interior, eventually facilitating their uptake into the cells composing the spheroids. Cellular apoptosis indicating programmed cell death was also observed in the HuH-7 spheroids treated with the PEGylated polyplexes, revealing that the observed growth inhibition was indeed induced by the RNAi of the RecQL1 siRNA. These data suggest that the smart PEGylated polyplexes can indeed penetrate into the multiple cell layers of 3D tumor masses in vivo, exerting therapeutic effects through the RNAi.

Introduction

The targeted delivery of small interfering RNAs (siRNAs)[1] is one of the major challenges in the field of cancer therapy through RNA interference (RNAi),[2] because siRNAs often tend to show low stability against enzymatic degradation, low permeability across the cell membrane, and preferential liver and renal clearance.[3] Therefore, the therapeutic value of siRNAs under in vivo conditions is largely dependent on the development of effective carrier systems which achieve modulated disposition in the body intravenously and accumulation in tumor tissues by enhanced permeability and retention (EPR) effect.[4] A promising strategy in this regard is the combination of PEGylation and carrier, namely a "smart" siRNA carrier (PEGylated polyplex) formulated through the supramolecular assembly (electrostatic interactions) of poly(L-lysine) (PLL) and lactosylated poly(ethylene glycol)-siRNA conjugate (Lac-PEG-siRNA) (Figure 1).[5] These smart PEGylated polyplexes, which have a size of approximately 100 nm, showed the high biocompatibility and enzymatic tolerability due to their segregated polyion complex core surrounded by a palisade of flexible and hydrophilic PEG layers. In particular, these smart PEGylated polyplexes with clustered lactose moieties on their periphery were successfully transported into the monolayer-cultured hepatic tumor cells by mediation of the asialoglycoprotein (ASGP) re-

[a] Prof. Dr. M. Oishi, Prof. Dr. Y. Nagasaki
Tsukuba Research Center for Interdisciplinary Materials Science (TIMS), University of Tsukuba, 1-1-1 Ten-noudai, Tsukuba, Ibaraki 305-8573 (Japan)
Fax: (+81) 29-853-5749
E-mail: nagasaki@nagalabo.jp

[b] Prof. Dr. K. Kataoka
Division of Clinical Biotechnology Center for Disease Biology and Integrative Medicine, Graduate School of Medicine, The University of Tokyo, 7-3-1 Hongo, Bunkyo-ku, Tokyo 113-0033 (Japan)

[c] Prof. Dr. Y. Nagasaki
Master's School of Medical Sciences, Graduate School of Comprehensive Human Sciences, University of Tsukuba, 1-1-1 Ten-noudai, Tsukuba, Ibaraki 305-8573, (Japan)

[d] Prof. Dr. N. Nishiyama, Prof. Dr. K. Itaka, Prof. Dr. K. Kataoka
Department of Materials Engineering, Graduate School of Engineering, The University of Tokyo, 7-3-1 Hongo, Bunkyo-ku, Tokyo 113-8656 (Japan)
Fax: (+81) 3-5841-7139
E-mail: kataoka@bmw.t.u-tokyo.ac.jp

[e] Dr. M. Takagi, Dr. A. Shimamoto, Dr. Y. Furuichi
GeneCare Research Institute Co., Ltd., 200 Kajiwara, Kamakura, Kanagawa 247-0063 (Japan)

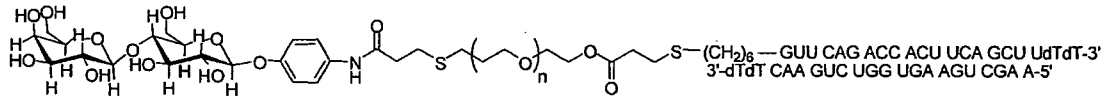

Figure 1. Chemical structure of the Lac-PEG-siRNA conjugate.

ceptor, inducing significant gene silencing of firefly luciferase (reporter gene) expression in monolayer-cultured HuH-7 cells at an extremely low siRNA concentration (IC_{50} = 1.3 nM). Therefore, the combination of this smart PEGylated polyplex system and a proper therapeutic siRNA is a promising approach to the creation of a systemic siRNA delivery system for the cancer therapy.

In this regard, siRNA-targeting DNA helicases are of particular interest. DNA helicases have recently been recognized to play important roles in DNA replication, recombination, repair, and transcription. Among many kinds of DNA helicases in living cells, the RecQ helicase family has been shown to have unique properties which are apparently involved in maintaining genomic stability. In humans, the RecQ helicase family has five members: RecQL1, BLM, WRN, RTS, and RecQL5.[6] BLM, WRN, and RTS are causative genes of Bloom syndrome, Werner syndrome, and a subset of Rothmund-Thomson syndrome, respectively, all of which are known to be recessive genetic disorders. Although RecQL1 is not yet known to have a relationship with any human disease, recent findings suggest that it is involved in the maintenance of the human genome.[7] LeRoy et al. have reported that RecQL1 helicase has Holliday junction branch migration activity, and the down-regulation of RecQL1 mRNA by RNAi resulted in an increase in sister chromatid exchange in human cells,[8] suggesting that RecQL1 helicase maintains the human genome by suppressing chromosomal recombination in the S phase. In addition, the RecQL1 protein was up-regulated by mitogenic stimulation or viral transformation in human B-lymphocytes,[9] suggesting that RecQL1 helicase is involved in genomic stabilization in growing cells such as cancer cells. Accordingly, RecQL1 helicase might be a good molecular target in cancer therapy.[10]

We would like to report herein, the significant and prolonged growth inhibition of hepatic multicellular tumor spheroids (MCTSs) by smart PEGylated polyplexes composed of PLL and Lac-PEG-siRNA conjugate bearing a RecQL1-siRNA segment. Note that MCTSs provide an in vivo tumor microenvironment characterized by high cell density, elevated interstitial pressure, hypoxia, and the existence of cell-cell contacts and a tumor extracellular matrix (ECM).[11] Apparently, these environmental factors play key roles in the diffusion, penetration, and growth-inhibitory effects of the siRNA-carriers in solid tumors in vivo. Therefore, using MCTSs, the efficacy of the siRNA delivery systems, including PEGylated polyplexes and lipoplexes, can be simply evaluated from the direct observation of the MCTS size; this method reflects the environmental factors characteristic of tumors and the direct gene silencing ability of the siRNA-carriers.

Results and Discussion

Design of the smart PEGylated polyplexes

Our strategy of formulating PEGylated polyplexes is based on the novel conjugation of siRNA with lactosylated PEG (Lac-PEG-siRNA), followed by complexation with poly(L-lysine) (PLL). The PEG-siRNA conjugates were synthesized according to our previously reported method;[5] the Michael addition of α-lactosyl-ω-acryl-PEG toward the 5'-thiol modified sense RNA to obtain Lac-PEG-single stranded RNA conjugate, followed by annealing with antisense RNA to prepare the Lac-PEG-siRNA conjugate through hybridization. A nonlactosylated conjugate, Ace-PEG-siRNA, was also prepared from the α-acetal-ω-acryl-PEG. The lactosyl-(lac-PEGylated polyplex) and nonlactosyl-(ace-PEGylated polyplex) PEGylated polyplexes were then prepared at an N/P ratio of 1 (=[amino group in polycation]/[phosphate group in siRNA segment]) by mixing the siRNA-PEG conjugates and PLL (degree of polymerization (DP) = 40, 100, or 460). The diameter of the PEGylated polyplex was determined to be approximately 110 nm by TEM.[5]

Growth inhibition of monolayer-cultured tumor cells by the PEGylated polyplexes

The elevation of RecQL1 expression has been positively correlated with various cancer cells, and the depletion of RecQL1 by siRNA complementary to RecQL1 mRNA dramatically inhibited cell proliferation and induced apoptosis in vitro and in vivo.[10] In contrast, the inhibition of the RecQL1 gene product in normal cells by RecQL1 siRNA induces no effect on cell proliferation, suggesting that RecQL1 siRNA is a potential therapeutic tool specific to the molecular targeting of cancer cells. To characterize the growth-inhibitory effect of the PEGylated polyplex system containing RecQL1 siRNA, an MTT assay was done using monolayer-cultured HuH-7 cells (human hepatoma cell) possessing asialoglycoprotein (ASGP) receptors, which recognize and internalize compounds bearing terminal lactose moieties.[12] As seen in Figure 2, almost no growth inhibition was observed for siRNA alone and conjugate alone even at a siRNA concentration of 150 nM in the presence of 10% fetal bovine serum (FBS). On the contrary, lac-PEGylated polyplex with PLL (DP = 100) showed 20% growth inhibition ($P^* < 0.05$) at 150 nM conjugate concentration. These results suggest that the lack of any growth-inhibitory effect on HuH-7 cells for free siRNA and free Lac-PEG-siRNA conjugate may be ascribed to the enzymatic degradation of the siRNA in the medium and to the impaired diffusivity of the negatively charged and hydrophilic free siRNA and Lac-PEG-siRNA conjugate through the negatively charged cell membrane. Significant growth inhibition was observed for the siRNA formulated with commercially

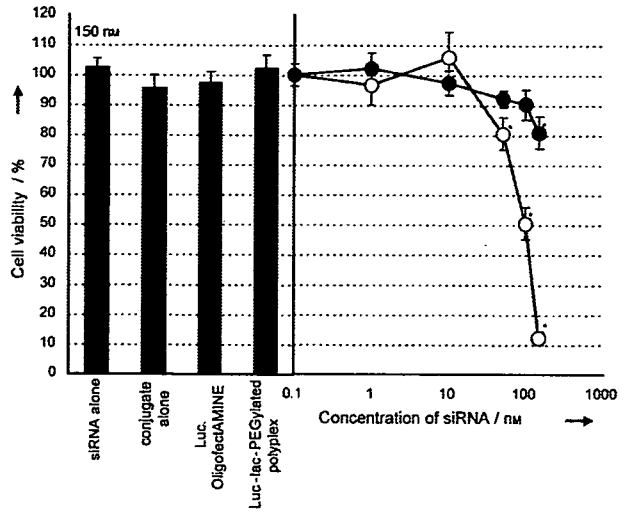

Figure 2. Growth inhibitory effect of the lac-PEGylated polyplexes (closed circles) and lipoplexes (open circles) from RecQL1 siRNA on monolayer-cultured HuH-7 cells. The cell viability was determined by means of an MTT assay after 96 h of incubation. The indicated concentrations of siRNA and conjugate are the final ones in the total transfection volume (250 μL). The plotted data are averages of triplicate experiments ±SD. The data points marked with asterisks are statistically significant compared with the mock data (buffer-treated cells) ($P^* < 0.05$).

available cationic lipid reagents, such as OligofectAMINE (lipoplex) (87% inhibition, $P^* < 0.05$). The lipoplex, which is cationic in character, may strongly interact with the negatively charged cell membrane leading to an appreciable increase in cellular uptake. It should be noticed that the lac-PEGylated polyplex and lipoplex, including luciferase-siRNA as a nontargeted sequence, induced no growth inhibition, strongly suggesting that the observed inhibitory effect against monolayer-cultured HuH-7 cells indeed occurred in a sequence-specific manner through RNAi based on the RecQL1-siRNA.

Growth inhibition of multicellular tumor spheroids (MCTS) by the PEGylated polyplexes

Although the efficacy of the siRNA formulated in the carrier systems in vitro has been generally evaluated by means of monolayer-cultured tumor cells, in vivo results to date have not always been in line with in vitro ones even if the carriers accumulated considerably in the tumor tissues because of the EPR effect. One plausible reason for this discrepancy may be that the monolayer assay only reflects the acute efficacy of the first several days, possibility overlooking the delayed or sustained siRNA action appearing at later stages. Furthermore, the diffusivity of the carriers into the 3D tumor tissue may be crucial in determining the in vivo efficacy, because hypoxic cells that are distant from blood vessels are relatively resistant to chemotherapy, causing the regrowth of the tumor; that is, there are tumor stem cells in the hypoxic regions of some tumors.[13] Therefore, alternatives to in vivo studies (animal experimentations), that is, appropriate in vitro models of in vivo solid tumors, are required to evaluate the prolonged efficacy of siRNA delivery systems, and to properly determine the diffusivity of siRNA-carriers into 3D tumor masses. Worth noting in this regard is the MCTS, which can be maintained in culture medium for many weeks with the physiological characteristics (microenvironment conditions) of in vivo 3D tumor tissues, such as high cell density, elevated interstitial pressure, hypoxia, the existence of cell-cell contacts, and ECM.[11] Indeed, the efficacy of gene delivery by cationic polyplexes and lipoplexes is limited because of their poor penetration ability into MCTSs.[14] Thus, MCTSs were used in this study as 3D in vitro tumor models for screening the growth-inhibitory effect of the siRNAs and their penetration ability into the spheroid interior.

RecQL1 siRNA-mediated growth inhibition of HuH-7 spheroids was assessed under the condition of prolonged culturing (up to 21 days). An HuH-7 spheroid with approximately 100 μm (75–100 μm) in diameter was initially used as the in vitro tumor model, because the maximum distance between the capillary blood vessels within avascular solid tumors is believed to be 200 μm or less.[15] As seen in Figure 3, no growth-inhibitory effect was observed for the siRNA alone or the Lac-PEG-siRNA conjugate alone, even at siRNA concentrations as high as 100 nM. These findings are consistent with the results obtained from the MTT assay using monolayer-cultured HuH-7 cells (Figure 2). In contrast, both the ace-PEGylated and lac-PEGylated polyplexes revealed a significant growth-inhibitory

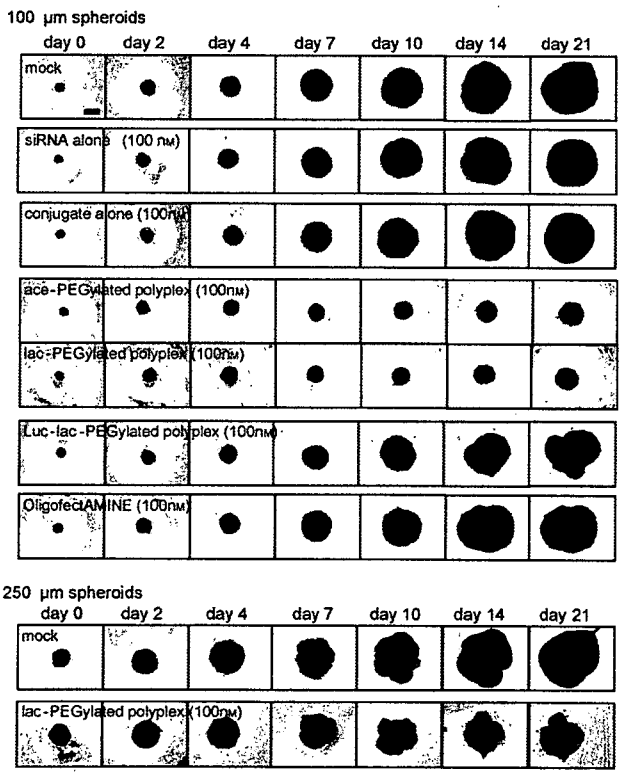

Figure 3. Phase-contrast images of the HuH-7 spheroids with an initial diameter of 100 μm and 250 μm (bar = 100 μm) treated with siRNA alone, Lac-PEG-siRNA conjugate alone, ace-PEGylated polyplex, lac-PEGylated polyplex, Luc-lac-PEGylated polyplex, and OligofectAMINE at concentrations of 100 nM.

effect in a dose-dependent manner (Figure 4a and b). In particular, the lac-PEGylated polyplexes exerted far more effective growth inhibition than the ace-PEGylated polyplexes at a conjugate concentration of as low as 10 nM; the 50% inhibitory concentration (IC_{50}) was determined to be 6 nM and 25 nM for the lac-PEGylated polyplex and ace-PEGylated polyplex, respectively (Figure 5). This almost fourfold increase in the growth-inhibitory effect exerted by lac-PEGylated polyplex is likely to be due to the facilitated uptake into the HuH-7 cells through an ASGP receptor-mediated endocytosis process.[5] This long-term growth-inhibitory effect (up to 21 days) on the spheroids by the single dose of PEGylated polyplexes added at the beginning is worth noting. The control lac-PEGylated polyplex, which included a siRNA against the firefly luciferase sequence (Luc-lac-PEGylated polyplex), induced almost no growth-inhibitory effect even at a conjugate concentration of 100 nM, strongly suggesting that the observed growth-inhibitory effect of the PEGylated polyplexes on the HuH-7 spheroids indeed occurred in a sequence-specific manner (Figure 3 and 4). Although the lipoplexes showed a higher growth-inhibitory effect than the PEGylated polyplex system on monolayer-cultured HuH-7 cells (Figure 2), almost no growth-inhibitory effect on the HuH-7 spheroids was observed even at a siRNA concentration of 100 nM (Figures 3 and 4a). This is presumably due to the cationic nature of the lipoplexes interacting nonspecifically with the negatively charged cell membrane and ECM, which leads to poor penetration into the HuH-7 spheroids. In addition, the spheroid size did not influence the growth-inhibitory effect of the PEGylated polyplexes; the lac-PEGylated polyplexes showed a significant growth-inhibitory effect on the HuH-7 spheroids with an initial diameter of both 200 (data not shown) and 250 μm (Figure 3), whereas the lipoplexes showed almost no growth-inhibitory effect even at high siRNA concentrations (100 nM).

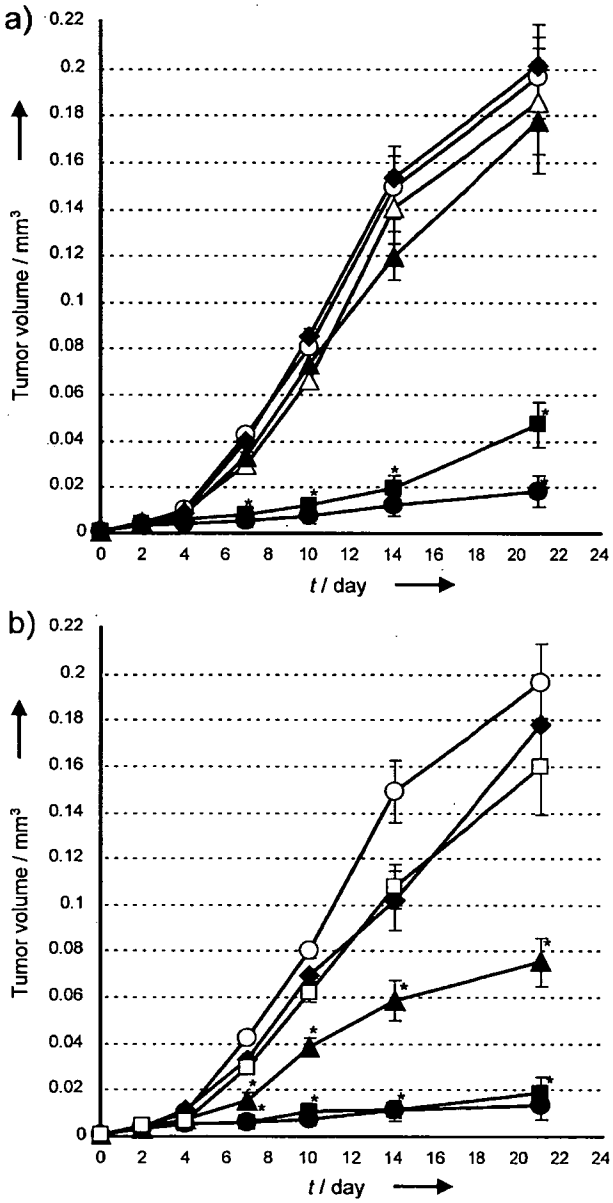

Figure 4. Time-dependent change in the volume of the spheroids treated with a) ace-PEGylated polyplexes and b) lac-PEGylated polyplexes; mock (open circles), OligofectAMINE at [siRNA] = 100 nM (open triangles), Luc-lac-PEGylated polyplex at [conjugate] = 100 nM (open squares), and the PEGylated polyplexes at [conjugate] = 100 nM (closed circles), 50 nM (closed squares), 10 nM (closed triangles), and 1 nM (closed lozenges). The volume of the spheroids was calculated as described in the Experimental Section. The data are averages of five HuH-7 spheroids ± SD. The data points marked with asterisks are statistically significant compared with the mock data (buffer-treated cells) ($P^* < 0.05$).

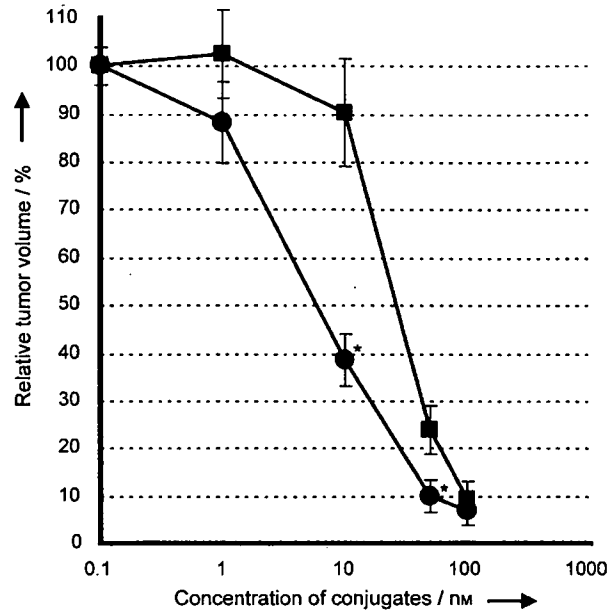

Figure 5. Effect of the complexed PEG-siRNA conjugate concentration on the growth inhibition of the HuH-7 spheroids with an initial diameter of 100 μm (closed squares: ace-PEGylated polyplexes; closed circles: lac-PEGylated polyplexes). The relative spheroid volume as the vertical axis was defined as the ratio of volume of the HuH-7 spheroids treated with PEGylated polyplexes to that of the mock sample on day 21. The data are averages of five HuH-7 spheroids ± SD. The data points for the lac-PEGylated polyplexes marked with asterisks are statistically significant compared with those for the ace-PEGylated polyplexes at the corresponding concentrations ($P^* < 0.05$).

Effect of the PLL length on the growth inhibition of spheroids by the PEGylated polyplexes

The effect of the PLL length on the growth inhibition of spheroids induced by the lac-PEGylated polyplexes was then examined. PLLs with varying DPs (40, 100, or 460) were used to prepare the PEGylated polyplex of the PEG-siRNA conjugate. As can be seen in Figure 6a, a striking effect of the PLL length on the growth inhibition of HuH-7 spheroids was observed at a conjugate concentration of 10 nM; the lac-PEGylated polyplexes prepared from shorter PLL (DP = 40) showed only limited efficacy relative to those from longer PLLs (DP = 100 or 460). Consequently, the IC_{50} was determined to be 7 nM, 6 nM, and 70 nM for the lac-PEGylated polyplexes prepared from PLL with DP = 460, DP = 100, and DP = 40, respectively (Figure 6b). These results indicate that the lac-PEGylated polyplexes formed from shorter PLL (DP = 40) are probably unstable under the extremely dilute conditions because of the critical dissociation phenomenon,[16] resulting in the impaired cellular uptake of the Lac-PEG-siRNA conjugate.

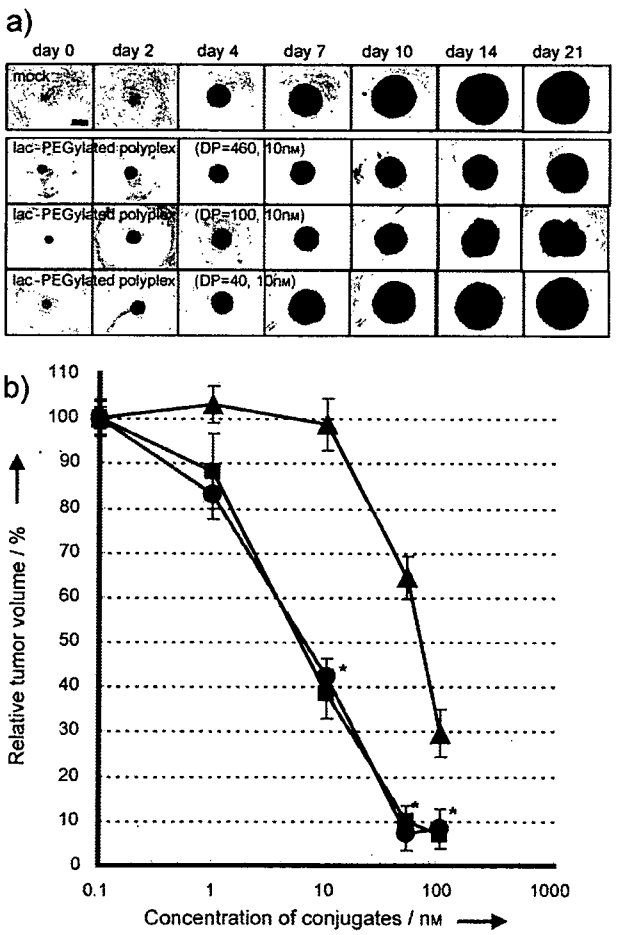

Figure 6. Effect of the PLL length on the growth-inhibitory effect of the lac-PEGylated polyplexes on the HuH-7 spheroids with an initial diameter of 100 μm (bar = 100 μm). a) Phase-contrast images of spheroids treated with the lac-PEGylated polyplexes composed of PLL with varying chain lengths. b) Change in the relative volume of the HuH-7 spheroids on day 21 with various concentrations of lac-PEGylated polyplexes composed of PLL with varying chain lengths (closed triangles: DP = 40; closed squares: DP = 100; closed circles: DP = 460). The relative spheroid volume as the vertical axis was defined as the ratio of volume of the HuH-7 spheroids treated with PEGylated polyplexes to that of the mock sample on day 21. The data are averages of five HuH-7 spheroids ± SD. The data points marked with asterisks are statistically significant compared with those for the lac-PEGylated polyplexes (DP = 40) at the corresponding concentrations ($P^* < 0.05$).

Distribution of the PEGylated polyplexes in multicellular tumor spheroids

To confirm whether or not the lac-PEGylated polyplex can effectively penetrate into the HuH-7 spheroids, 5′-FITC-labeled (fluorescein isothiocyanate) oligodeoxynucleotide (ODN) having the same antisense sequence as the firefly luciferase siRNA was hybridized with the sense firefly luciferase PEG-ODN conjugate to form an FITC-labeled Lac-PEG-dsODN conjugate. The FITC-labeled conjugate was mixed with PLL (DP = 100) at an N/P ratio of 1 to form a PEGylated polyplex with the FITC-label (FITC-PEGylated polyplex). An FITC-labeled lipoplex was also prepared by mixing the OligofectAMINE with FITC-labeled dsODN having the same sequence as the firefly luciferase siRNA. The fluorescence of the FITC-labeled lipoplexes and the FITC-PEGylated polyplexes was observed under a confocal fluorescence-scanning microscope after 48 h of incubation as shown in Figure 7. Most of the fluorescence from the FITC-labeled lipoplexes was seen only at the periphery of the HuH-7 spheroid even after 48 h of incubation (Figure 7a), indicating that the lipoplexes have a poor ability to penetrate into the HuH-7 spheroids, presumably due to the large complex size and the strong interaction with the negatively charged cell membrane and/or ECM.[17] This poor penetration of the lipoplexes into the HuH-7 spheroids obviously has a negative effect on the RecQL1 siRNA-mediated growth inhibition. In sharp contrast, the fluorescence from the FITC-PEGylated polyplexes was observed not only at the periphery but also much

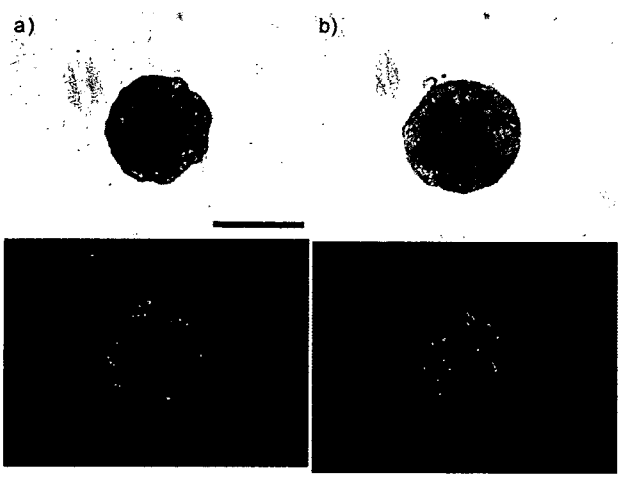

Figure 7. Distribution in the HuH-7 spheroids of the a) FITC-labeled dsODN in the OligofectAMINE lipoplexes (z-axis: 87 μm) and b) FITC-labeled Lac-PEG-dsODN conjugate in the lac-PEGylated polyplexes (z-axis: 79 μm) after 48 h of incubation. Initial diameter of the spheroids: 100 μm (bar = 200 μm).

